In: Wagner W., Székely, B. (eds.): ISPRS TC VII Symposium – 100 Years ISPRS, Vienna, Austria, July 5–7, 2010, IAPRS, Vol. XXXVIII, Part 7B

Contents   Author Index   Keyword Index

SIMULATED RAIN RATE EFFECTS ON SAR INTERFEROGRAMS

A. Elmzoughi[1], R. Abdelfattah[1,2] and Z. Belhadj[1]

[1] URISA, École Supérieure des Communications, Tunis, Route de Raouède Km 3.5, 2083, Tunisia .
[2] Département ITI, Telecom Bretagne, Institut TELECOM, CS 83818 - 29238 Brest Cedex 3 - France
Email: riadh.abdelfattah@supcom.rnu.tn and ziad.belhadj@supcom.rnu.tn

Commission TC VII

KEY WORDS: InSAR, Atmospheric effects, Interferograms, Signal delay.

ABSTRACT:

In this paper we discuss influence of the rain rate on SAR interferograms. Calculations of the path delay for different rain rate intensities was made by considering a physical model for the rain drops and applying the Rayleigh approximation. The calculations do not include estimations of the delay due to the melting layer of precipitations and due to the precipitating cloud above the melting layer since they could be neglected. On simulated examples of interferograms considering perfectly flat areas, we show that there is a strong increase in a propagation delay associated with rain rate and that, the rain can induce a considerable propagation delay of several centimeters.

1 INTRODUCTION: INTERFEROMETRY AND ATMOSPHERIC EFFECTS

ERS1 and ERS2 provide 2D measurements of the earth surface with a high resolution of 4×20 m. The phase value of every resolution cell is defined as a superposition of the term which corresponds to the geometric distance, a term which corresponds to propagation effects, ψ_{prop}, and the term which represents the scattering within the resolution cell. By creating an interferogram, effectively the phases corresponding to two measurements are subtracted from each other and if objects within resolution cells did not move and did not change from one acquisition to the other, the differential phase is mainly defined by the propagation effects and the difference in observation geometries. Furthermore, if a reference elevation model is available one can remove the topographic phase component. The remaining phase would fully be determined by the propagation through the ionosphere, $\Delta\psi_{iono}$, and atmosphere, $\Delta\psi_{atm}$ (Zebker et al., 1994):

$$\begin{aligned} \Delta\psi_{prop} &= \Delta\psi_{iono} + \Delta\psi_{atm} \\ &= \Delta\psi_{iono} + (\Delta\psi_{hydr} + \Delta\psi_{wet} + \Delta\psi_{liquid}) \end{aligned} \quad (1)$$

Indeed, the atmospheric component in its turn depends on hydrostatic part, propagation through the dry atmosphere, wet delay, propagation through water vapor and liquid part, caused by propagation through volume filled with liquid droplets.

The hydrostatic and ionospheric parts are dominating the delay signal, but they hardly vary over the interferogram and may easily be removed from the rest of the signal. The wet part, caused by propagation throw a volume filled with liquid particles, have a stochastic spatial behavior and therefore it is more difficult to compensate for them (Moissev et al., 2002).

In this paper we will discuss influence of rain on the atmospheric phase delay. Calculations of the path delay for different rain rate intensities was made by considering a physical model for the rain drops and applying the Rayleight approximation. Then in order to illustrate our study, some interferograms were generated and discussed.

2 SIMULATED SIGNAL DELAY INDUCED BY THE RAIN DROPS

2.1 The physical model

For radar applications there is a great agreement that raindrops can be well approximated by oblate spheroids (Nelson and Gokhale, 1972) characterized by their axis ratio e. In the literature, a great number of theoretically derived relations between the axis ratio and the equivolume sphere diameter D were derived (Imai, 1950) (Spilhaus, 1948). Most of these relations are describing the equilibrium shape (shape of the rain drop in absence of perturbation). However, the derived axis ratio from a linear fit to the wind-tunnel data of Pruppacher and Beard (Pruppacher and Beard, 1970) represents a very useful one:

$$e = 1.03 - 0.062 \times D. \quad (2)$$

The Drop Size Distribution (DSD) represents the number of particles that have the same equivalent diameter and noted $N(D)$ located in a volume of $1m^3$. Based on extensive measurements, Marshall and Palmer proposed a single-parameter negative exponential relation in (Marshall and Palmer, 1948):

$$N(D) = 8000 \times exp(-\wedge D), \quad (3)$$

where the spherical equivalent diameter D is in mm and $\wedge$ is the parameter of the exponential distribution function which can be related to the rain rate throw the following equation:

$$\wedge = 4.1/R^{0.21}, \quad (4)$$

where R is given in mm/hr.

An other important physical parameter for the rain drops is their complex dielectric constant since it is related to transmission, absorbtion and backscattering phenomenons. It depends principally in the exiting wavelength (water activity) and the temperature. Evaluated for a wavelength of 5.6 cm (which corresponds to the ERS1/2 wavelength) and at $10°$c the dielectrical constant can be approximated by (Marshall and Palmer, 1948):

$$\epsilon \simeq 70 + 30i \quad (5)$$

In: Wagner W., Székely, B. (eds.): ISPRS TC VII Symposium – 100 Years ISPRS, Vienna, Austria, July 5–7, 2010, IAPRS, Vol. XXXVIII, Part 7B

Contents　　　　　　　　Author Index　　　　　　　　Keyword Index

where $i = \sqrt{-1}$.

2.2 Phase delay computing

It was shown in (Oguchi, 1983) that for the case of coherent prop-agation in rain the propagation phase delay, δ in mm/km, can be calculated as:

$$\delta = 10^{-3} \frac{2\pi}{k^2} \int Re(f(D))N(D)dD, \qquad (6)$$

where k is the wave number (corresponding to a wavelength of 56 mm for the case of ERS1/2) and $f(D)$ is the forward scattering amplitude in mm and $N(D)$ is in $mm^{-1}m^{-3}$.

In this case $f(D)$ can be evaluated using Rayleigh approximation (Bringi and Chandrasekar, 2001). The scattered amplitude for h-polarized incidence wave can be then calculated as:

$$f(D) = \frac{k^2}{24} D^3 (\epsilon - 1) \Lambda, \qquad (7)$$

where ϵ is the relative permittivity of water and Λ is given by:

$$\Lambda = \frac{1}{1 + \lambda_1(e - 1)}, \qquad (8)$$

where

$$\lambda = \frac{1-\lambda_2}{2} \quad \text{and} \quad \lambda_2 = \frac{1+f^2}{f^2}\left(1 - \frac{1}{f}tan^{-1}(f)\right), \qquad (9)$$

where

$$f = e^{-2} - 1. \qquad (10)$$

As we can conclude the expression of $Re(f(D))$ is very com-plicated and cannot be used directly for deriving an analytical expression for the phase delay related to the rain. Thus more suitable expressions are needed.

In order to overcome this problem, we have simulated the for-ward scattering amplitude for D ranges between 1 and 8 mm. we have fixed the temperature at 10^{oc} and the wavelength at 5.6 cm. In these conditions, the value of ϵ can be approximated by 70 + 30j. Then, for a given value of D, the corresponding axis ratio e is computed using equation 2. Then, $f(D)$ is computed using equa-tions 3 and 5-11. From the resulting curve of the real part we can derive a powerless relation between $Re(f(D))$ and D that have the forme αD^β. Coefficients α and β are estimated by the non linear regression algorithm. For our simulation $\alpha = 3.7 \times 10^{-4}$ and $\beta = 3.02$. Figure 1 shows the good agreement between the Rayleigh approximation and the powerless one.

After replacing $Re(f(D))$ by its powerless expression and per-forming some simple mathematical manipulations equation 6 be-comes:

$$\begin{aligned} \delta &= \frac{8\lambda^2\alpha\wedge^{-\beta}}{2\pi} \int D^\beta \exp(-D)dD \\ &= \frac{8\lambda^2\alpha\wedge^{-\beta}}{2\pi}\Gamma(\beta) \end{aligned}, \qquad (11)$$

where $\Gamma(\cdot)$ is the gamma function.

Finally a simple expression relating the phase delay to the rain rate can be derived using equation 4 as:

$$\delta = \frac{8\lambda^2\alpha 4.1^{-\beta}R^{0.21\beta}}{2\pi}\Gamma(\beta). \qquad (12)$$

The path delay for different rain intensities were calculated. It should be noted that raindrop diameter is usually truncated at 8
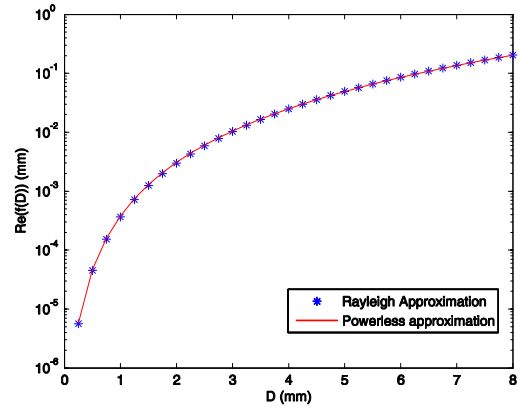
Figure 1: Fitting Rayleigh approximation to a powerless one.

mm, since particles with a larger diameter are unstable. In Figure 2 the result of these calculations is given. It can be seen that for high rain intensities the path delay can be as high as several centimeters.
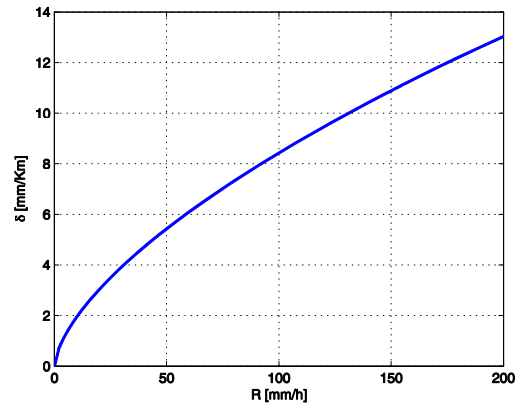
Figure 2: Path delay as a function of the rain rate.

3 SIMULATED INTERFEROGRAMS

Our simulation for this work consists in generating two interfero-grams for a perfectly flat area. The first one was generated with-out taking into consideration any rain effects and the second one takes into a consideration a layer of rain that covers the imaged area. Figure 3 and 4 show the considered computation geometry.

3.1 Computing geometry

In figure 3, $\overrightarrow{B}$ designates the baseline vector, θ the incidence angle, T the radar swath and r_1 and r_2 are ranges between a fixed point in the imaged area and the position of the radar for the first and the second acquisition respectively. In the absence of rain $\Delta\psi_{prop}$ depends only in r_1 and r_2 (Abdelfattah and Nicolas, 2002):

$$\Delta\psi_{prop} = \frac{4\pi}{\lambda}(r_2 - r_1). \qquad (13)$$

Thus, rain free interferogram can be directly generated using r_1 and r_2. If we consider the configuration of figure 3 and after performing some geometrical manipulations we can deduce that:

$$\begin{aligned} r_1 &= \sqrt{x^2 + y^2 + H^2} \\ r_2 &= \sqrt{(x - B_x)^2 + (y - B_y)^2 + (H + B_z)^2} \end{aligned} \qquad (14)$$

In: Wagner W., Székely, B. (eds.): ISPRS TC VII Symposium – 100 Years ISPRS, Vienna, Austria, July 5–7, 2010, IAPRS, Vol. XXXVIII, Part 7B

Contents   Author Index   Keyword Index

for

$$x \in [H\tan(\theta) - \tfrac{T}{2}, H\tan(\theta) + \tfrac{T}{2}]$$
$$y \in [-\tfrac{T}{2}, \tfrac{T}{2}]$$

Now, let consider the configuration with the presence of a rain layer of figure 4. h designates the hight of the rain layer and r_{1r} and r_{2r} are ranges between a fixed point in the imaged area and the intersection points of r_1 and r_2 with the top of the rain layer respectively. r_{1r} and r_{2r} corresponds exactly to the path crossed by the radar signal throw the rain medium. Also, r_{1r} and r_{2r} can be computed using some simple geometrical manipulations. Here we avoided to give expressions of r_{1r} and r_{2r} for reasons of clarity. Let R_1 and R_2 the rain rates corresponding to the first and the second acquisition respectively. The phase difference due to propagation throw the rain is then :

$$\Delta\psi_{prop-r} = r_{2r} \times \delta(R_2) - r_{1r} \times \delta(R_1). \qquad (15)$$

and the total phase difference, from which the rain contaminated interferogram is computed, is:

$$\Delta\psi = \Delta\psi_{prop} + \Delta\psi_{prop-r}. \qquad (16)$$

It should be noted that these calculations do not include estimations of the delay due to the melting layer of precipitations and due to the precipitating cloud above the melting layer. However, we expect that contribution of the melting layer is rather limited since it occupies the limited height range (usually in the order of few hundred meters). The precipitating cloud on the other hand can have a rather large height range, but due to the fact that the relative permittivity of ice is much smaller than the one of water the contribution of the precipitating cloud to the signal delay would be negligible.

3.2 Interferograms generation and discussion

In order to simulate interferograms we have fixed the configuration parameters to be equal to the ERS 1/2 radar ones. Table 1 shows their values.

Parameter	Simulation value
H	785 Km
θ	23°
λ	56 mm
T	10 Km
$\vec{B}$	[10 10 100]m
Pixel Resolution	50×50m
h	10 Km

Table 1: simulation parameters

Note that the rain was considered to be uniform, with the same rain rate, for the hole area. Figure 5 shows resulting phase delay (in cm) for different rain rates. From these results, we can conclude that there is a strong increase in a propagation delay associated with rain rate and that, the rain can induce a considerable propagation delay of several centimeters. Also we can verify by these results that the rain induced phase delay presents very small variation between the nearest and the most far point in the imaged area. Therefor, in these conditions, the rain induced phase delay can be considered as constant all over the imaged zone. Thus its effect on the interferogram will be a simple translation of the fringes. This fact is clear in figure 6 which shows the rain-free and some rain-contaminated interferograms. As expected, interferograms for the area, considered to be perfectly flat, consists in a succession of parallel fringes. The amount of the fringes
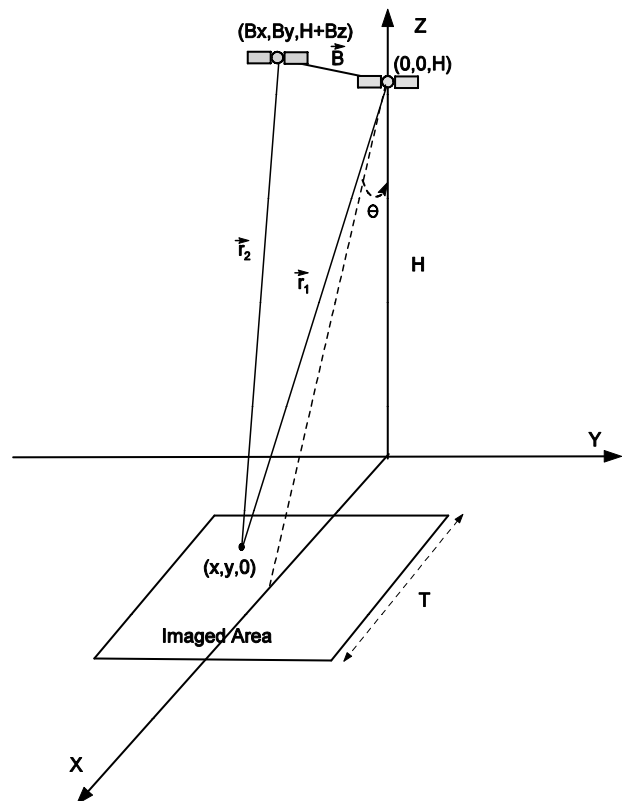
Figure 3: Geometry used for Insar computations for a flat area in the absence of rain.

transition can be deduced by dividing the rain induced delay by $\lambda/2$. For example, light rain with 5mm/hr induce a transition of approximately half a fringe. We can easily verify this result by comparing the rain-free and the rain-contaminated interferograms.

4 CONCLUSION

In this paper we discussed the influence of the rain rate on SAR interferograms. Calculations of the path delay for different rain rate intensities was made by considering a physical model for the rain drops and applying the Rayleight approximation. The calculations do not include estimations of the delay due to the melting layer of precipitations and due to the precipitating cloud above the melting layer since they could be neglected. Simulated examples of interferograms considering perfectly flat areas were generated and showed that there is a strong increase in a propagation delay associated with rain rate and that, the rain can induce a considerable propagation delay of several centimeters causing translation of interferogram's fringes.

REFERENCES

Abdelfattah, R. and Nicolas, J.M., 2002. Topographic SAR interferometry formulation for high-precision DEM generation, *IEEE Transaction on Geoscience and Remote Sensing*, vol. 40, NO. 11, pp. 2415-2426.

Bringi, V.N. and Chandrasekar, V., 2001. Polarimetric Doppler Weather Radar. Principles and Applications, *1st ed. Cambridge, U.K.: Cambridge Univ. Press.*

8

In: Wagner W., Székely, B. (eds.): ISPRS TC VII Symposium – 100 Years ISPRS, Vienna, Austria, July 5–7, 2010, IAPRS, Vol. XXXVIII, Part 7B

Contents   Author Index   Keyword Index
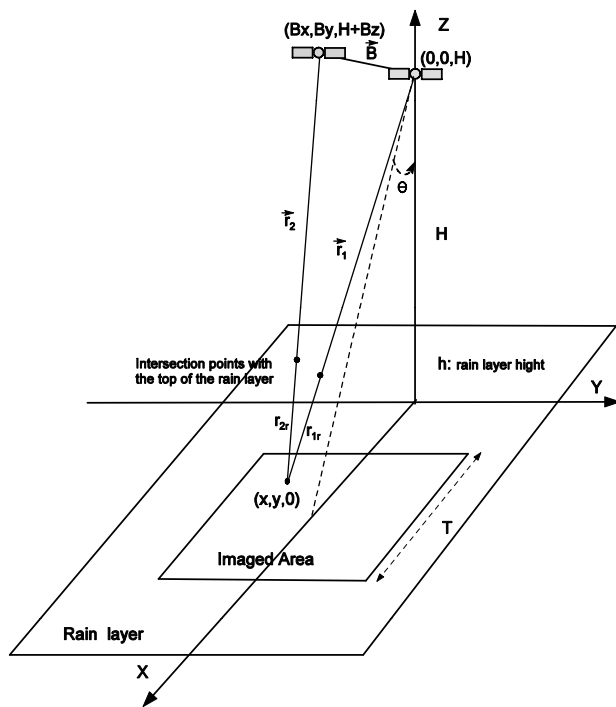
Figure 4: Geometry used for Insar computations for a flat area in the presence of rain.

Imai, I., 1950. On the velocity of falling drops, *Geophys. Mag.,* vol. 21, pp. 244-249.

Marshall, J.S. and Palmer, W.M., 1948. The distribution of raindrops with size, *J. Meteorol.,* vol. 5, pp. 165-166.

Moisseev, D.N., Hanssen, R.F. and van Leijen, F.J., 2002. Water vapor observations with SAR, microwave radiometer and GPS: comparaison of scaling characteristics, *Proc. of the 6nd European Conference on Radar Meteorology*, Delft, The Netherlands.

Nelson, A.R. and Gokhale, N.R., 1972. Oscillation frequencies of freely suspended water drops, *J. Geophy. Res.,* vol. 77, pp. 2724-2727.

Oguchi, T., 1983. Electromagnetic wave propagation and scatterin in rain and other hydrometeors, *Proc. IEEE,* vol. 71, pp.1029-1077.

Pruppacher, H.R. and Beard, K.V., 1970. A wind tunned investigation of the internal circulation and shape of water drops falling at terminal velocity in air, *Quart. J. R. Met. Soc.,* vol. 96, pp. 247-256.

Spilhaus, A.F., 1948. Rain drop size, shape and falling speed, *J. Meteorol.,* vol. 5, pp. 108-110.

Zebker, H.A., Werner, C.L., Rosen, P.A. and Hensley, R.S., 1994. Accuracy of topographic maps derived from ERS-1 interferometric radar, *IEEE Transaction on Geoscience and Remote Sensing*, vol. 32, pp. 823-836.
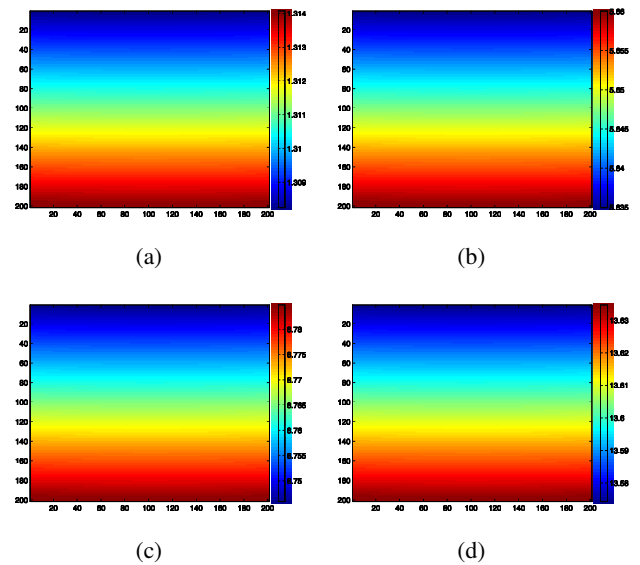
Figure 5: Rain induced signal delay (in cm) for a rain rate of(a)5 mm/h (b) 50 mm/h (c) 100 mm/h (d) 200 mm/h.
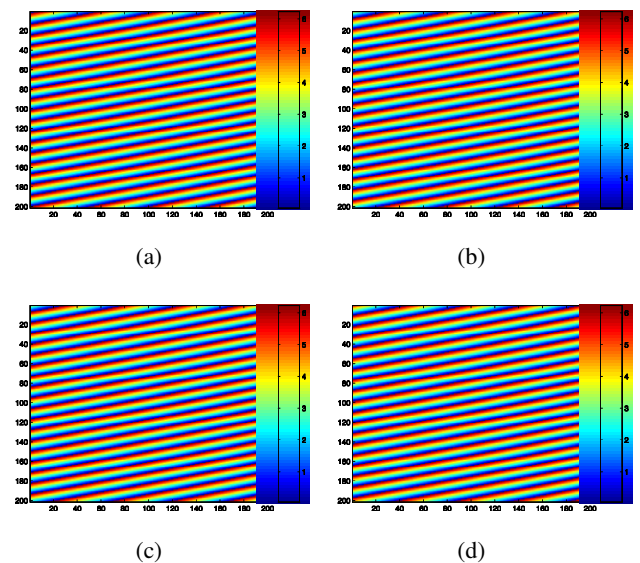
Figure 6: Resulting interferograms (a) rain free (b) 5 mm/h (c) 50 mm/h (d) 100 mm/h.